Jurnal Kejuruteraan 37(6) 2025: 3023-3033
https://doi.org/10.17576/jkukm-2025-37(6)-36

Optimizing Process Parameters in Direct Laser Metal Deposition of Ti-6Al-4V for Single-Layer Track Formation: Influence on Deposition Geometry

Jailani Jamaludin[a,b,c*], Mohd Azlan Suhaimi[c], Safian Sharif[c] & Abdul Hamid Ahmad[c]

[a]*School of Engineering, University of Wollongong Malaysia, Glenmarie Campus, Jalan Kontraktor U1/14, Glenpark U1, 40150 Shah Alam, Malaysia*

[b]*School of Engineering, UOW Malaysia KDU Penang University College, Jalan Anson, 10400 George Town, Pulau Pinang, Malaysia*

[c]*Faculty of Mechanical Engineering, Universiti Teknologi Malaysia, 81310 Johor Bahru, Johor, Malaysia*

[*]*Corresponding author: jailani.j@uow.edu.my*

Received 4 December 2024, Received in revised form 29 May 2025
Accepted 29 June 2025, Available online 30 September 2025

ABSTRACT

The growing demand for high-quality metal components has exposed the limitations of conventional manufacturing techniques. Direct Laser Metal Deposition (DLMD), a key metal additive manufacturing method, offers promising capabilities but its reliability is often compromised by dimensional inconsistencies linked to melt pool anomalies. Although prior studies have explored general process optimization, there remains a critical gap in understanding how specific parameters impact geometrical stability. Hence, this study addresses these issues by investigating the effects of process parameters specifically overlap ratio and travel speed under an oscillation scanning strategy to enhance geometrical reliability in DLMD deposits specifically for single layer track. Nine experimental runs were conducted using a Taguchi design to evaluate dimensional accuracy, focusing on absolute deviation from the target deposition height (1.5 mm) and standard deviation of deposition width (3.0 mm). Surface geometry metrics were analysed using signal-to-noise (SN) ratios and ANOVA analyses. Results reveal that travel speed significantly influences both height and width consistency, with optimal values identified at 450 mm/min and 800 mm/min, respectively. Overlap ratio also affects deposition geometry, with 70% producing the most stable outcomes across both metrics. Revised ANOVA confirms the statistical significance of travel speed, while overlap ratio exhibits a weaker but notable effect. Pareto analysis further underscores travel speed as the dominant factor governing melt pool dynamics and thermal input. The findings demonstrate that precise control of travel speed is essential for achieving consistent deposition profiles, while overlap ratio serves as a secondary tuning parameter. These insights support improved process control in DLMD, enabling enhanced dimensional accuracy and repeatability in advanced manufacturing applications.

Keywords: Direct Energy Deposition (DED); Direct Laser Metal Deposition (DLMD); Additive manufacturing (AM); Ti-6Al-4V; parameters optimization

INTRODUCTION

Direct Energy Deposition (DED) offers a transformative approach to additive manufacturing by enabling the direct fabrication of complex three-dimensional structures from digital models, distinguishing it fundamentally from traditional welding and cladding techniques. Within the broader category of DED, direct laser metal deposition (DLMD) utilizes a concentrated energy source, typically a laser to melt metallic powder, facilitating the layer-wise construction of components (Mazzarisi et al. 2023; Mehrabi et al. 2023; Moradi et al. 2023; Pellizzari et al. 2022; Rezaee Hajideh & Farahani, 2024; Shang et al. 2022)the effective parameters in the Direct Laser Metal Deposition Method (DLMD. Figure 1 presents an illustration of the DLMD technique employed in this study.

This technology presents multiple advantages, with recent research placing particular emphasis on its application in component repair. underscored its suitability for the aeronautical sector, especially when employing Ti-6Al-4V alloy (Gradl 2021). On the other hand, the findings by Rauch et al. (2020)so that the repaired component can provide the same level of service than a new one. This paper focuses on the repair of Ti-6Al-4V parts by powder based LMD AM and investigates its accuracy, repeatability and reliability. At first, an experimental campaign has been carried out to evaluate the characteristics of as-built material. Optimal process parameter selection is made by a porosity and macrostructure analysis. Tensile properties, Low Cycle Fatigue and crack propagation studies have been done on as-built samples (100% AM highlighted the mechanical characteristics of the metal deposition specimens, with a particular emphasis on interface properties. These properties demonstrate promising potential not only for repair applications but also for the fabrication of fully functional components. Their investigation examined factors such as bonding quality, microstructural integrity, and load-bearing capacity. Since its emergence, DLMD has gained traction as a focal point of research within the domain of laser-based additive manufacturing. Its versatility has enabled widespread application across diverse fields, including mechanical engineering, biomedical device fabrication, military defense systems, and beyond.

Despite its advantages, DLMD faces notable challenges, particularly when processing superalloys. High thermal gradients and accelerated cooling induce residual stresses and grain boundary segregation, contributing to solidification cracking, as observed by Moradi et al. (2022). Another study by Bidare et al. (2022)additive manufacturing of these alloys is particularly challenging. In this paper, the influence of process parameters on the porosity, crack formation and microstructure of additively manufactured CM247LC nickel-based alloy is analysed. The feasibility of the direct laser deposition (DLD highlighted the sensitivity of microstructure to laser deposition parameters. High laser power in deposition improves sample density but can cause solidification cracks due to rapid cooling. These findings highlight the imperative of refining process parameters to address solidification stage to preserve the structural integrity of superalloys.

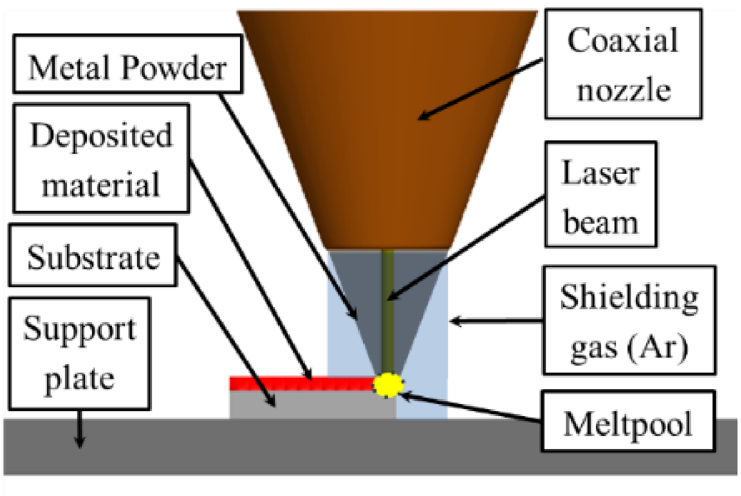

FIGURE 1. DLMD process

On the other side, the resulting clad geometry must also comply with the standard dimensional requirements. A previous study from Ermurat et al. (2013) investigates parameters such as high power laser, laser focal distance, travel speed, feeding gas flow rate, and standoff distance affect the geometry of a single clad. The findings reveal that a smaller clad geometry is achieved when the gas flow rate, travel speed, and standoff distance are set at higher levels, and the laser focal spot size is minimized. In support of this, Mazzarisi et al. (2022)based on laser cladding, which focuses mainly on 3D manufacturing applications. DLMD allows the production of thin-walled components by overlaying single-track depositions. Several issues can affect the deposition process and compromise the flatness of the surface on which subsequent tracks will be deposited. This work focused on deposition troubles simulated by means of a designed variation of the standoff distance and the laser defocusing distance. The effects of these two important process parameters on the deposition process were investigated. The experimental tests were performed by depositing a nickel-based superalloy powder on AISI 304 stainless steel plates through a coaxial nozzle. The work was carried out using an ytterbium fiber laser source and a deposition head equipped with an advanced and innovative motorized optics system. This allows the decoupled variation of the laser defocusing distance and consequently the laser spot size on the substrate surface with respect to the standoff distance. Results showed an influence of standoff distance and laser defocusing distance on the geometrical characteristics of the clad, such as clad width, clad height, penetration depth, and dilution. An experimental setup consisting of a light coaxial to the powder flow and a laterally positioned camera was designed to investigate the spatial powder distribution. Moreover, an analytical model for the powder distribution and clad width were proposed and validated. The analysis of variance (ANOVA demonstrated that variations in laser defocusing markedly affect clad characteristics, including width, height, and penetration depth.

Additionally, Mahamood et al. (2012) investigated the use of Ti6Al4V powder and substrate materials, reporting that higher laser power leads to increased track width and deposition efficiency. While the height of the deposited material initially rises with increasing laser power, it subsequently declines due to an effect attributed to greater dilution, which promotes deeper penetration into the substrate. Meanwhile, the layer height increases linearly with rising powder flow rate (Bennett et al. 2017; Lee et al. 2017; Srivastava et al. 2000). Subsequently, Moradi et al. (2021) concluded that lowering the traverse speed enhances the interaction between the laser beam and powder particles, thereby increasing both the height and width of the resulting wall structures. These observations collectively indicate that key process parameters namely laser power, powder flow rate, and traverse speed have significant influence on the geometry of the deposited material.

Further investigation into the process parameters revealed that the geometry of the deposited material is primarily governed by the size and shape of the melt pool. Variations in parameters such as laser power, powder flow rate, and traverse speed significantly influence melt pool morphology. Consequently, a scanning strategy focused on optimizing the laser spot size was explored. Among the methods introduced, Franco (2017) and Aversa et al. (2022) proposed an oscillation-based strategy to enhance deposition quality. The deposition geometry is strongly influenced by overlap ratio and travel speed, both of which govern the thermal distribution and melt pool behavior. Building on this approach, Ahmad et al. (2025) utilized trochoidal oscillation to enhance the resolution and consistency of deposition studies. The finding shown the method enhance substrate deformation and surface flatness, with optimal results achieved using narrower path widths for multilayer deposition. Theirs studies, demonstrated the effectiveness of oscillatory movement strategies based on overlapping values. However, their methodology was specifically applied to multilayer deposition, not single layer track deposition.

Building on the promising outcomes by addressing a critical gap of the initial strategy, this study undertook a more detailed investigation focused specifically on single layer track deposition. It explores the coupled effects of overlap ratio and travel speed on deposition geometry within an oscillatory scanning framework, where a configuration that remains underexplored in existing literature for single layer track applications. While previous research has broadly acknowledged the influence of thermal input on melt pool behavior, this work uniquely quantifies how controlled variation in overlap ratio and travel speed governs the deposition geometry on single layer track. By linking these parameters to measurable outcomes such as bead geometry, the study introduces a refined process control framework that enhances dimensional reliability.

Regarding on that matter, a low overlap ratio results in narrow, highly concentrated energy input zones that can induce deep, unstable melt pools. These deep pools, while providing strong penetration, are prone to defects such as vapor-induced porosity and inconsistent bead geometry. Conversely, a high overlap ratio distributes energy more uniformly across the scan path, promoting stable conduction-mode melting characterized by wider and shallower melt pools, smoother bead surfaces, and improved dimensional consistency. Meanwhile, the travel speed further modulates energy density which can be explained by slower speeds increase dwell time and can enlarge the melt pool, potentially causing overheating or distortion, while faster speeds may lead to insufficient fusion or poor surface finish due to reduced energy absorption.

In conclusion, this study strategically optimizes the overlap ratio and travel speed during the oscillation scanning process to regulate melt pool behavior, enabling precise control over deposition geometry and consistent interlayer bonding specifically for single layer track. This, in turn, ensures reliable part quality, supports longer product lifespans and reduces waste. The refined process parameters promote scalable, low-waste additive manufacturing, aligning with circular economy principles and advancing sustainable production practices across high-impact industries.

METHODOLOGY

EXPERIMENT DESIGN AND PROCEDURE

Key parameters for successful deposition were identified, with critical benchmarks including laser scanning speed, powder feed rate, and laser power. To refine deposition outcomes, additional parameters governing oscillatory motion which are overlap ratio and travel speed were systematically configured. A set of nine experimental runs was conducted to investigate the effects of these input conditions on selected output metrics, primarily focusing on geometrical deposition for single-track formation. Table 1 summarizes the experimental conditions employed.

TABLE 1. Design Matrix of Oscillation Parameters

Factors	Acronym	Unit	Level
Overlap ratio	OL	%	50 / 70 / 90
Travel speed	V_{osc}	mm/min	100 / 450 / 800

TABLE 2. Elemental Profile of Ti-6Al-4V Powder

Factors	Weight %	Weight % σ	Atomic %
Aluminium	5.247	0.264	8.975
Titanium	90.206	0.600	86.907
Vanadium	4.547	0.570	4.119

Regarding material selection, Ti-6Al-4V powder was deposited onto a Ti-6Al-4V substrate measuring using the DLMD method. The powder's elemental composition and particle morphology were analyzed using a scanning electron microscope (Hitachi S-3400N), with results detailed in Table 2. The powder utilized in this study was fabricated via gas atomization, yielding predominantly spherical particles with occasional satellite formations on their surfaces. Particle diameters ranged between 10 µm and 60 µm. The substrate, machined to dimensions of 20 mm × 10 mm × 3 mm using wire-cut Electrical Discharge Machining (EDM), served as the deposition base.

EXPERIMENT EQUIPMENT

For the Direct Laser Metal Deposition (DLMD) process, a 1.5 kW fiber laser integrated with a laser cladding head (model LT-CH002A) was employed as shown in Figure 2.

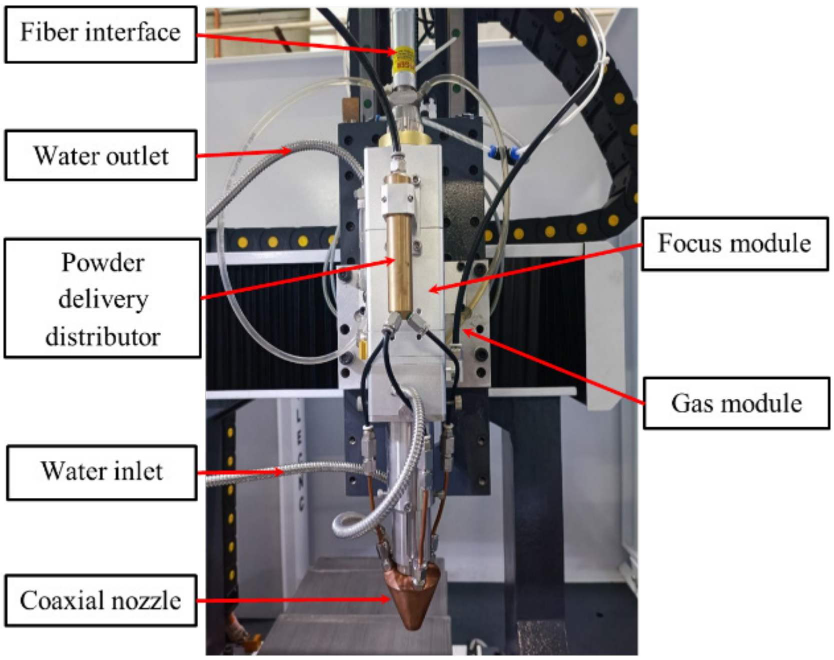

FIGURE 2. LT-CH002A Cladding head.

The setup featured a 3 mm laser spot size, a vertical focal distance of 15 mm, and a 50 mm clear aperture. A coaxial nozzle configuration facilitated uniform powder delivery onto the substrate (Gabor et al. 2022). Powder flow was directed through three annular channels, converging into the powder concentration zone located 15–20 mm beneath the nozzle tip. The cladding head was powered by a Raycus RFL-C1500X laser fiber unit, operating continuously at a wavelength of 1080 nm. A complete listing of fixed process parameters is presented in Table 3 while Figure 3 shows the equipment configuration for DLMD machine.

TABLE 3. Standardized Input Conditions

Variables	Unit	Value
Laser power	W	450
Laser spot diameter	mm	3
Laser focal distance	mm	15
Laser focal length	mm	300
Laser wavelength	nm	1080
Powder particle size	µm	10 - 60
Powder deposition rate	g/min	3.5
Substrate dimension	mm	10 x 20 x 3
Argon gas flow rate (Shielding)	litre/min	10
Argon gas flow rate (Carrier)	litre/min	3

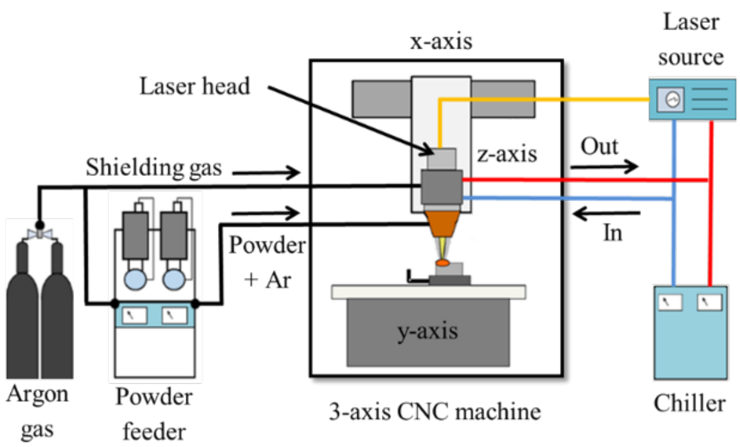

FIGURE 3. DLMD Equipment Configuration and Schematic Overview

SAMPLE PREPARATIONS

Preliminary experiments demonstrated successful deposition using a laser power of 450 W, a scanning speed of 100 mm/min, and a powder feed rate of 3.5 g/min. These parameters, optimized for straight-line deposition in single-layer tracks, served as the foundation for subsequent trials. Building upon this baseline, an oscillation strategy was implemented to further improve deposition characteristics. This approach required the careful selection of two critical input parameters: overlap ratio and travel speed, as presented in Table 1 previously.

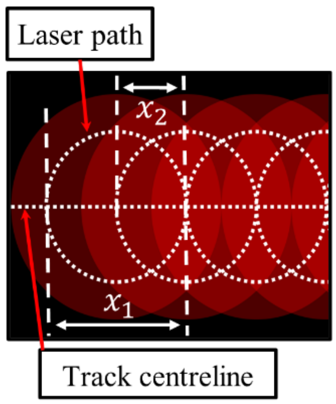

FIGURE 4. Oscillatory Laser Scanning Pattern

Overlap ratio was defined by the radial displacement between successive cycles of the laser's circular motion, measured from the centerline outward. Figure 4 shows the laser scanning pattern for oscillation strategy. The calculation and corresponding overlap value were determined using Eq. 1. The example in Eq. 2 illustrates the computation for an overlap level (OL) of 50%.

$$OL = \frac{x_2}{x_1} \times 100 \tag{1}$$

$$OL = \frac{x_2}{x_1} \times 100 = \frac{1.5\text{mm}}{3\text{mm}} \times 100 = 50\% \tag{2}$$

As the oscillation strategy employs circular motion, the deposition rate is directly affected by the velocity of this movement which define by travel speed in Table 1 above. For each experimental configuration, a single sample was produced and subjected to an identical analytical procedure to ensure consistency in results.

The sample was then subsequently ground using 600, 1200, and 2000 grit abrasives, followed by polishing with a cloth pad. Microscopic observations were conducted using an optical microscope (XOPTRON XST150). The geometric dimensions of the deposition, including average width and height, were analyzed using i-Solution software. The measurements obtained are presented in Figure 5.

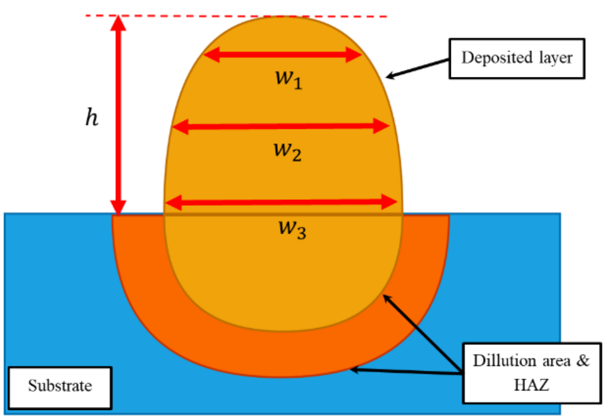

FIGURE 5. Schematic of Deposition Geometry Evaluation Process.

For the deposition height, absolute deviation was use which predetermine height was set based on ideal deposition target. For deposition width, standard deviation was used which measured the amount of variation or dispersion of set value. A low standard deviation indicates that the values tend to be close to the mean, while a high standard deviation shows that the values are spread out over a wider range. Hence, the SD should be low of the value indicating nearest to the targeted specification. Eq. 3 present the AD function and Eq. 4 present the SD function calculating value for geometry of the AM sample. The value of h is the measured value while the h_r is the reference targeted value. The different is the AD of the measured height. Smaller the number indicate closest to the targeted height. For the measurement of the width, w_i is a one-point value along the three region width of AM sample, w_r is the targeted value of the width of AM sample and N is the number of measured point of the AM sample.

$$AD = |h - h_r| \tag{3}$$

$$SD = \sqrt{\frac{\sum (w_i - w_r)^2}{N}} \tag{4}$$

Figure 6 displays the measured sample of deposition geometry with an overlap ratio (OL) of 50% and a travel speed (V_{osc}) of 100 mm/min.

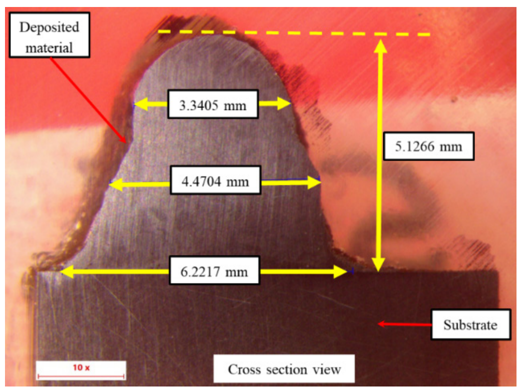

FIGURE 6. Sample Cross-Section View (OL = 50%, Vosc = 100 mm/min).

RESULTS AND DISCUSSION

All nine experimental runs were conducted using the DLMD process under controlled conditions to ensure consistency. Figure 7 captures the actual printing process. To enhance powder flowability during transport through the powder delivery system, Ti-6Al-4V metal powder was preheated to 70 °C. All experiments were performed within the same environmental setting to minimize variability and ensure repeatability. Table 4 summarizes the average geometrical metrics of the AM sample, including the absolute deviation of height and the standard deviation of width. All experimental output results were analyzed using the Taguchi method. The corresponding ANOVA and Pareto chart analyses for each output parameter are presented separately.

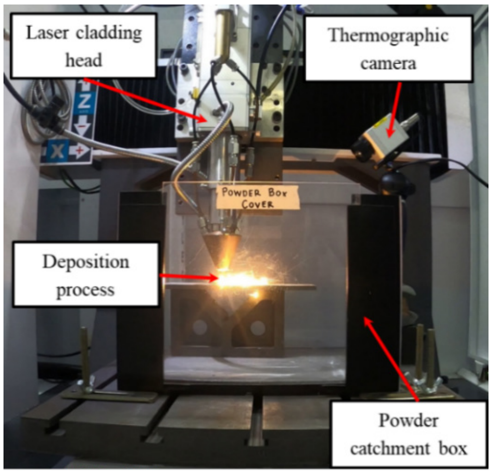

FIGURE 7. DLMD printing process.

TABLE 4. Results overview.

No.	Input parameters			
	Overlapping ratio (%)	Travel speed (mm/min)	AD Deposition Height (mm)	SD Deposition width (mm)
			Target: 1.5mm	Target: 3.0mm
1	50	100	3.63	2.05
2	50	450	0.41	1.17
3	50	800	0.90	1.09
4	70	100	5.84	1.70
5	70	450	0.06	1.17
6	70	800	0.53	1.02
7	90	100	13.00	2.61
8	90	450	3.05	1.33
9	90	800	1.62	1.09

In general, the highest signal-to-noise (SN) ratio reflects the optimal combination of input parameters that minimize variability and enhance consistency in the deposition process. For deposition height, the smaller-the-better criterion is applied, where reduced absolute deviation signifies superior performance. Similarly, for the standard deviation of the average deposition width, minimal variation relative to the target width of 3 mm is considered ideal. Figure 8 presents two separate main effects plots illustrating the SN ratios for deposition height and deposition width. Each plot highlights the influence of individual parameters on process consistency with the criteria applied independently to height and width metrics.

The analysis reveals the optimal combination of input parameters that minimizes absolute deviation from the target height of 1.5 mm in Figure 8(a). In this context, a higher SN ratio signifies reduced variability and improved consistency in achieving the desired dimensional outcome. Among the tested overlap ratios, the 70% level yields the highest SN ratio, indicating superior performance in maintaining deposition height close to the target with minimal deviation. The SN ratio for travel speed peaks at 450 mm/min, suggesting that this speed facilitates the most uniform deposition height. The combination of 70% overlap ratio and 450 mm/min travel speed demonstrates the most effective parameter set for minimizing absolute deviation and ensuring dimensional accuracy in the deposition height.

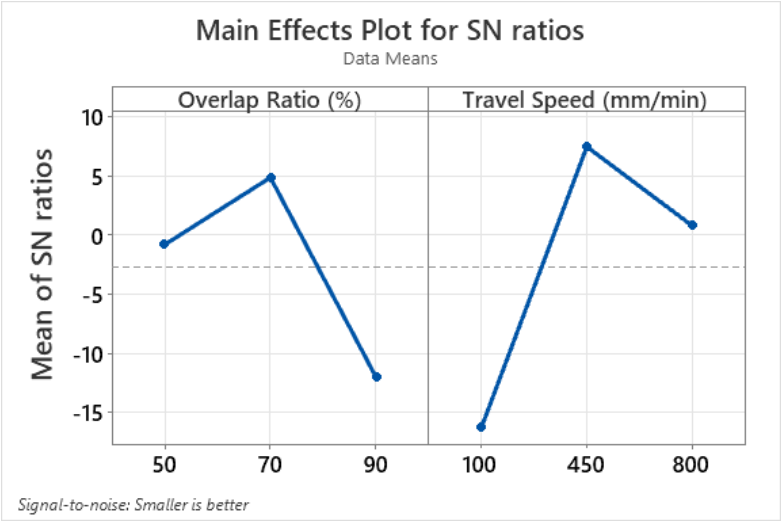

(a)

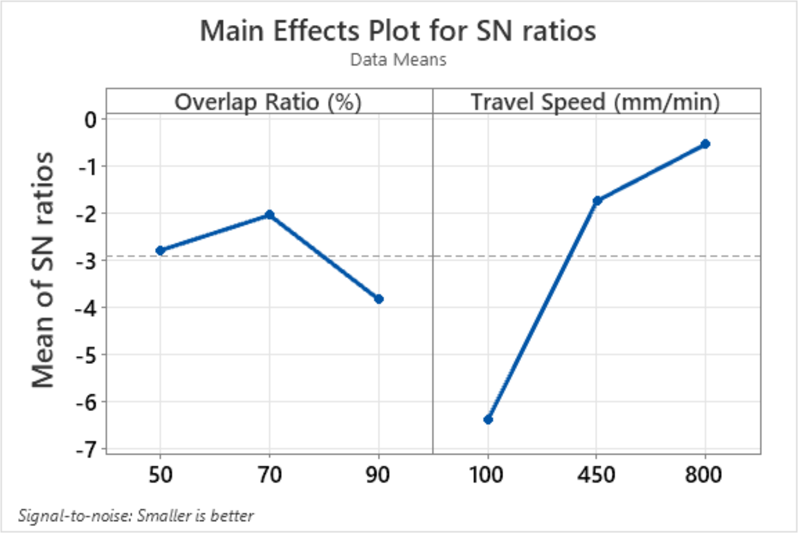

(b)

FIGURE 8. SN ratio plots for (a) absolute deviation of deposition height and (b) standard deviation of deposition width.

Meanwhile, Figure 8(b) focuses on the standard deviation of the average deposition width, with a target dimension of 3 mm. The main effects plot reveals that the overlap ratio of 70% yields the highest SN ratio among the tested levels and this setting most effectively minimizes deviation from the target width. For travel speed, the SN ratio increases progressively from 100 mm/min to 450 mm/min and continues to rise at 800 mm/min, with the highest value observed at 800 mm/min. This trend suggests that higher travel speeds contribute to more consistent deposition width. Therefore, the optimal parameter combination for minimizing variation in deposition width is a 70% overlap ratio paired with a travel speed of 800 mm/min.

The overlap ratio determines how much each successive pass overlaps with the previous one, thereby affecting the heat accumulation and material buildup in the deposition zone (Ocylok et al. 2014; Wu et al. 2022). Insufficient overlap leads to poor fusion between adjacent tracks, resulting in inconsistent material deposition and increased geometric variability while high overlap causes excessive reheating and remelting of previously deposited material, which can lead to overbuilding, distortion, and unstable deposition profiles due to thermal saturation and fluid instability. Meanwhile, travel speed governs the interaction time between the heat source and the substrate, which in turn affects the thermal input per unit length and the cooling rate. At low speeds prolonged exposure leads to excessive heat input, causing wider melt pools and increased fluid mobility, which can result in uncontrolled spreading and height buildup. This contributes to greater deviation in both height and width. At high speeds, the heat input is reduced, leading to narrower and more stable melt pools, which favour consistent width formation but may compromise height uniformity due to insufficient material deposition.

TABLE 5. Revised ANOVA deposition height.

Source	DF	SS	MS	F-Value	P-Value
Regression	2	89.91	44.955	5.88	0.039
Overlap Ratio (%)	1	27.02	27.016	3.53	0.109
Travel Speed (mm/min)	1	62.89	62.894	8.22	0.029
Error	6	45.90	7.650		
Total	8	135.81			

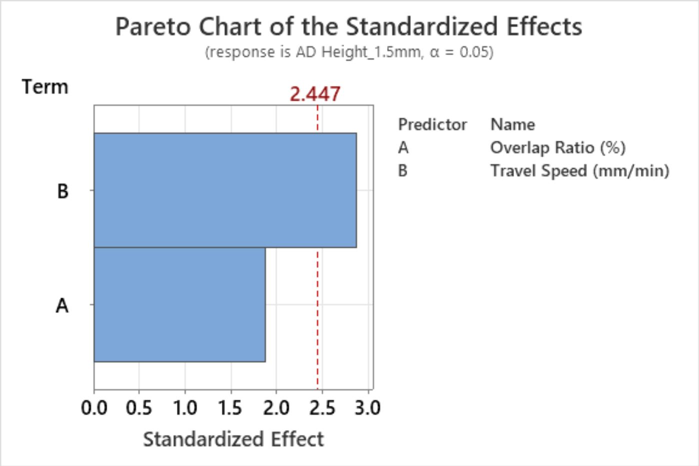

FIGURE 9. Pareto chart deposition height.

The revised ANOVA results presented in Tables 5 and 6 confirm that the regression models for both deposition height and width are statistically significant, indicating that the combined influence of overlap ratio and travel speed plays a meaningful role in shaping deposition geometry. Notably, travel speed exhibits a strong individual effect, with a p-value of 0.029 for deposition height and 0.007 for deposition width, both below the conventional significance threshold. This impact is likely attributed to the direct relationship between travel speed and thermal input where slower speeds increase laser dwell time, resulting in greater energy absorption, deeper melt pools, and increased vertical buildup. Conversely, higher speeds reduce energy input per unit length, limiting melt pool depth and lateral spread, which directly affects both height and width of the deposition.

TABLE 6. Revised ANOVA deposition width.

Source	DF	SS	MS	F-Value	P-Value
Regression	2	1.76111	0.88055	8.38	0.018
Overlap Ratio (%)	1	0.08389	0.08389	0.80	0.406
Travel Speed (mm/min)	1	1.67721	1.67721	15.96	0.007
Error	6	0.63049	0.10508		
Total	8	2.39159			

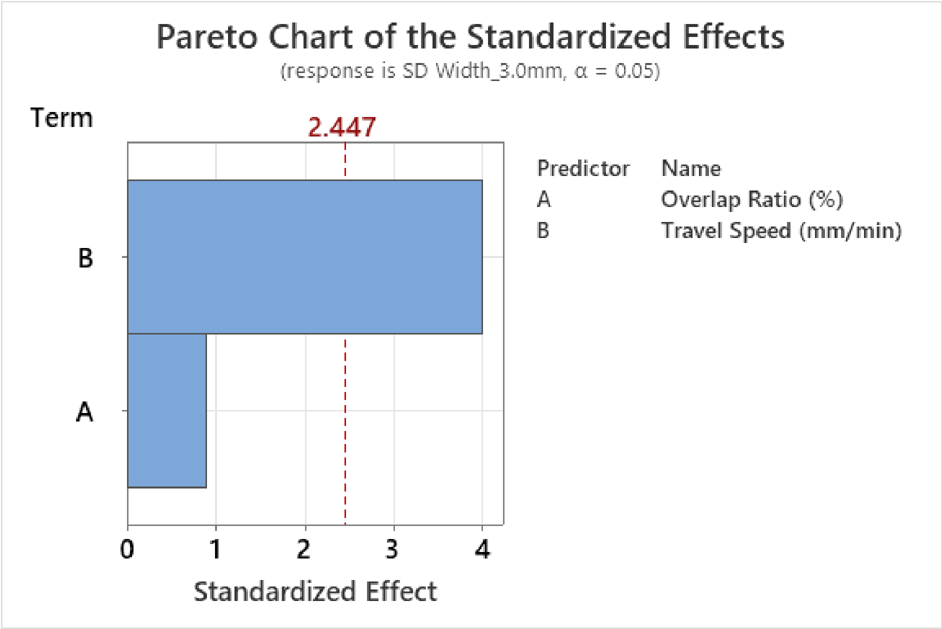

FIGURE 10. Pareto chart deposition width.

In contrast, the overlap ratio shows less influence on both geometric outputs. This may be due to its secondary role in energy distribution which does not substantially alter the localized thermal gradient in a single pass especially when the laser power and powder feed rate are held constant. The Pareto charts of standardized effects for deposition height (targeted at 1.5 mm) in Figure 9 and width (targeted at 3.0 mm) in Figure 10 provide strong visual confirmation of the ANOVA results. In both cases, travel speed surpasses the reference significance threshold, indicating a statistically significant effect on the output responses. This reinforces the ANOVA finding that travel speed is the most influential process parameter. Its pronounced impact on deposition geometry substantiates its critical role in modulating melt pool dynamics, influencing thermal gradients, and governing solidification rates. These effects collectively contribute to the dimensional accuracy and consistency of the deposited features, validating the robustness of the statistical model and the physical relevance of the identified trends.

CONCLUSION

The study systematically evaluated the influence of overlap ratio and travel speed on the geometrical consistency of DLMD deposits, focusing on absolute deviation in deposition height and standard deviation in deposition width specifically for single layer track. Through Taguchi-based analysis and regression modeling, the findings reveal that travel speed is the dominant factor affecting both dimensional metrics. In contrast, overlap ratio exhibits a comparatively weaker influence, likely due to its secondary role in thermal energy distribution under constant laser power and powder feed conditions. The optimal parameter combinations identified are:

1. For deposition height: 70% overlap ratio and 450 mm/min travel speed
2. For deposition width: 70% overlap ratio and 800 mm/min travel speed

These settings minimize deviation from target dimensions (1.5 mm height and 3.0 mm width), as confirmed by signal-to-noise (SN) ratio plots and supported by ANOVA and Pareto chart analyses. The results underscore the critical role of thermal input modulation via travel speed in controlling melt pool behavior, solidification dynamics, and ultimately, geometric fidelity.

ACKNOWLEDGEMENT

This research is fully supported by Universiti Teknologi Malaysia under grant No: Q.J130000.4351.09G66 and partial financial support from UOW Malaysia. Their support has made this important research viable and effective.

DECLARATION OF COMPETING INTEREST

The authors declare no competing interests.

REFERENCES

Ahmad, A. H., Suhaimi, M. A., Sharif, S., Jamaludin, J., & Zakaria, K. 2025. Experimental investigation and optimization of trochoidal tool paths as an alternative to linear scanning patterns for enhanced build quality in direct laser metal deposition. *The International Journal of Advanced Manufacturing Technology* 138(3): 1055–1073. https://doi.org/10.1007/s00170-025-15557-0

Aversa, A., Carrozza, A., Marchese, G., Felicioni, S., De Chirico, M., Lombardi, M., Bondioli, F., & Fino, P. 2022. Productivity Enhancement in Directed Energy Deposition: The Oscillating Scanning Strategy Approach. *Metals and Materials International*, *0123456789*. https://doi.org/10.1007/s12540-022-01356-9

Bennett, J. L., Wolff, S. J., Hyatt, G., Ehmann, K., & Cao, J. 2017. Thermal effect on clad dimension for laser deposited Inconel 718. *Journal of Manufacturing Processes* 28: 550–557. https://doi.org/10.1016/j.jmapro.2017.04.024

Bidare, P., Mehmeti, A., Jiménez, A., Li, S., Garman, C., Dimov, S., & Essa, K. 2022. High-density direct laser deposition (DLD) of CM247LC alloy: Microstructure, porosity and cracks. *International Journal of Advanced Manufacturing Technology* 120(11–12): 8063–8074. https://doi.org/10.1007/s00170-022-09289-8

Ermurat, M., Arslan, M. A., Erzincanli, F., & Uzman, I. 2013. Process parameters investigation of a laser-generated single clad for minimum size using design of experiments. *Rapid Prototyping Journal* 19(6): 452–462. https://doi.org/10.1108/RPJ-06-2011-0062

Franco, F. 2017. *Wobbling Laser Beam Welding of Copper*. NOVA University Lisbon.

Gabor, T., Yun, H., Akin, S., Kim, K. H., Park, J. K., & Jun, M. B. G. 2022. Continuous coaxial nozzle designs for improved powder focusing in direct laser metal deposition. *Journal of Manufacturing Processes* 83(September): 116–128. https://doi.org/10.1016/j.jmapro.2022.08.039

Gradl, P. R. 2021. Principles of directed energy deposition for aerospace applications. In *Drive AM Industry Connect W.M. Keck Center for 3D Innovation* (Issue February). https://doi.org/10.13140/RG.2.2.10504.75527

Lee, E. M., Shin, G. Y., Yoon, H. S., & Shim, D. S. 2017. Study of the effects of process parameters on deposited single track of M4 powder based direct energy deposition. *Journal of Mechanical Science and Technology* 31(7): 3411–3418. https://doi.org/10.1007/s12206-017-0239-5

Mahamood, R. M., Akinlabi, E. T., Shukla, M., & Pityana, S. 2012. Effect of laser power on material efficiency, layer height and width of laser metal deposited Ti6Al4V. *Lecture Notes in Engineering and Computer Science* 2: 1433–1438.

Mazzarisi, M., Angelastro, A., Latte, M., Colucci, T., Palano, F., & Campanelli, S. L. 2023. Thermal monitoring of laser metal deposition strategies using infrared thermography. *Journal of Manufacturing Processes* 85(October 2022): 594–611. https://doi.org/10.1016/j.jmapro.2022.11.067

Mazzarisi, M., Errico, V., Angelastro, A., & Campanelli, S. L. 2022. Influence of standoff distance and laser defocusing distance on direct laser metal deposition of a nickel-based superalloy. In *International Journal of Advanced Manufacturing Technology* 120(3–4): 2407–2428. https://doi.org/10.1007/s00170-022-08945-3

Mehrabi, O., Hossein Seyedkashi, S. M., & Moradi, M. 2023. Experimental and response surface study on additive manufacturing of functionally graded steel-inconel wall using direct laser metal deposition. *Optics and Laser Technology* 167(July): 109707. https://doi.org/10.1016/j.optlastec.2023.109707

Moradi, M., Hasani, A., Pourmand, Z., & Lawrence, J. 2021. Direct laser metal deposition additive manufacturing of Inconel 718 superalloy: Statistical modelling and optimization by design of experiments. *Optics and Laser Technology* 144(March): 107380. https://doi.org/10.1016/j.optlastec.2021.107380

Moradi, M., Kornokar, K., Nematzadeh, F., Mostaan, H., Meiabadi, S., Demers, V., & Lawrence, J. 2023. Microstructural and mechanical investigation on fiber laser welding of S500MC steel. *Sadhana - Academy Proceedings in Engineering Sciences* 48(1). https://doi.org/10.1007/s12046-023-02079-2

Moradi, M., Pourmand, Z., Hasani, A., Karami Moghadam, M., Sakhaei, A. H., Shafiee, M., & Lawrence, J. 2022. Direct laser metal deposition (DLMD) additive manufacturing (AM) of Inconel 718 superalloy: Elemental, microstructural and physical properties evaluation. *Optik* 259(March): 169018. https://doi.org/10.1016/j.ijleo.2022.169018

Ocylok, S., Alexeev, E., Mann, S., Weisheit, A., Wissenbach, K., & Kelbassa, I. 2014. Correlations of melt pool geometry and process parameters during laser metal deposition by coaxial process monitoring. *Physics Procedia* 56(C): 228–238. https://doi.org/10.1016/j.phpro.2014.08.167